Early time dynamics of strongly coupled ultracold neutral Ca^+ and Ca^{2+} plasmas

M. Lyon* and S. D. Bergeson

Department of Physics and Astronomy, Brigham Young University, Provo, UT 84602, USA

For interacting many-body systems the two most natural energy scales are the average energy per particle and the average nearest-neighbor potential energy. When the ratio of the nearest-neighbor potential energy to the kinetic energy is greater than 1, we say that the system is "strongly coupled," where strong coupling is characterized by the parameter Γ. This dimensionless parameter describes the complete thermodynamic state of a system, making it possible to study the fundamental behavior of strongly coupled systems as manifested in high energy-density plasmas using low energy table-top experiments. In our experiments, we are working with plasmas in this exotic regime. In this paper we report on the progress of an experiment in laser-cooled calcium designed to increase the strong coupling of an ultracold neutral plasma by promoting the plasma ions to the second ionization state. We report preliminary measurements of the change in the Ca^+ ion temperature due to the second ionization.

I. Introduction

Ultracold neutral plasmas provide fertile ground for investigating the properties of strongly coupled systems. Such systems include the interior of white dwarf stars and some Jovian planets, the crusts of neutron stars, high density laser-produced plasmas, and laser-driven fusion plasmas. This is because plasma evolution occurs on the time scale of the inverse plasma frequency, ω_p^{-1}, where the ion plasma frequency is $\omega_p = (ne^2/m_i\epsilon_0)^{1/2}$ [1–4]. For high temperature, high density plasmas, this time scale is on the order of femto- or attoseconds. The much colder and relatively less dense ultracold plasmas evolve on the microsecond time scale, which makes it possible to study the plasma characteristics and evolution directly using commonly employed techniques of atomic physics.

The thermodynamic properties of strongly coupled plasmas depend only on the dimensionless parameter Γ. This parameter, called the strong coupling parameter, is given by the ratio of the nearest neighbor Coulomb potential energy to the average kinetic energy of the ions

$$\Gamma = \frac{e^2}{4\pi\epsilon_0 a_{\rm ws}} \frac{1}{k_{\rm B} T_{\rm i}}, \qquad (1)$$

where e is the fundamental charge, $a_{\rm ws} \equiv (3/4\pi n)^{1/3}$ is the Wigner-Seitz radius or the average distance between ions and n is the plasma density, $k_{\rm B}$ is Boltzman's constant, and $T_{\rm i}$ is the ion temperature. By scaling Γ we can learn something about the fundamental behavior of strongly coupled systems. Since the thermodynamic properties of strongly coupled plasmas depend only on Γ, plasmas that may differ by orders of magnitude in temperature and/or density share many of the same characteristics. Experiments in the laboratory with ultracold plasmas thus allow us to probe strongly coupled Coulomb systems similar to those found in astrophysical environments and created in high energy research laboratories using a table top apparatus.

The goal of this research is to study the dynamics of ultracold neutral plasmas in a coupling regime not currently described by classical plasma physics models. However, the degree of strong coupling in an ultracold plasmas is limited by a process called disorder-induced heating (DIH). Ultracold plasmas are typically created by photoionizing neutral atoms in a magneto-optical trap (MOT). When an ultracold plasma is created in a MOT, the random spatial distribution of the neutral atoms gives rise to spatially uncorrelated ions. Ions move to minimize the excess electric potential energy they have due their spatial disorder, thus increasing their kinetic en-

* mary_lyon@byu.edu

ergy and decreasing the strong coupling. Past work has shown that DIH scales with the density of the plasma and the electron temperature [5].

A recent simulation predicted that higher values of the strong coupling parameter in ultracold neutral plasmas can be realized if the plasma ions are excited to higher ionization states [6]. The maximum value of Γ depends on the time at which the second ionization laser pulses arrive. We have built an experiment in laser-cooled calcium designed to test this prediction and increase the strong coupling of an ultracold neutral plasma by promoting the plasma ions to the second ionization state. This paper reports on the progress and recent results of that experiment.

II. Experiment

A. Cooling and trapping in the MOT

Approximately 20 million calcium atoms are laser-cooled and trapped in a MOT [7] using a 423 nm laser tuned to the $4s^2\ {}^1S_0 \rightarrow 4s4p\ {}^1P_1^{\rm o}$ resonance transition in calcium. The trapping laser beam is generated by amplifying and frequency doubling a 846 nm diode laser. An optical frequency comb from a mode-locked femtosecond laser is used to lock the trapping laser to the appropriate resonance transition. Then, we detune the 423 nm trapping light one atomic linewidth (approximately 35 MHz) below resonance using an acousto-optic modulator (AOM).

The calcium atoms are produced by a temperature controlled oven that heats bulk calcium into an atomic vapor. The atoms leave the oven through a narrow nozzle, which creates an atomic beam. A laser beam directed opposite the atomic beam slows the atoms down and increases the loading rate of the MOT. This "slowing" laser beam is detuned several linewidths below the 423 nm atomic resonance. A 672 nm "repump" laser pumps atoms that fall into the metastable $4s3d\ {}^1D_2$ state back into the ground state via the highly excited $4s5p\ {}^1P_1$ state. With the slowing laser beam and repump laser this experiment typically achieves peak MOT densities on the order of 10^{10} cm^{-3} and temperatures of approximately 1 mK.

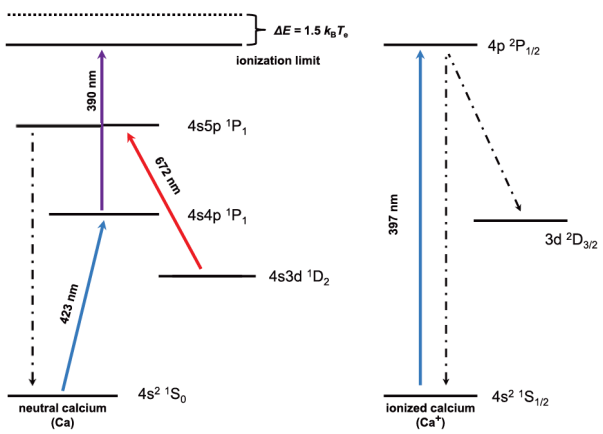

FIG. 1. Partial energy level diagram for Ca (left) and Ca^+ (right). Cooling and trapping of the neutral Ca uses the 423 nm transition. The first ionization is a two photon process with laser pulses at 423 nm and 390 nm. Laser-induced fluorescence measurements are made using a cw probe laser tuned to the 397 nm transition.

B. Generating an ultracold neutral Ca plasma

Once the calcium atoms are trapped, they are photoionized using a two-photon ionization process. This ionization is achieved using two copropagating 3 ns pulse lasers at 423 nm and 390 nm. These lasers drive the $4s^2\ {}^1S_0 \rightarrow 4s4p\ {}^1P_1^{\rm o}$ transition and the $4s4p\ {}^1P_1^{\rm o} \rightarrow$**continuum**, respectively. Adjusting the wavelength of the 390 nm laser (which drives the transition into the continuum) varies the initial energy of the electrons in the plasma, because the excess photon energy above the ionization limit is carried away by the electrons.

C. Measurements using laser-induced fluorescence

After the plasma is produced, measurements are made using laser-induced fluorescence generated by a probe laser tuned below the 397 nm $4s\ {}^2S_{1/2} \rightarrow 4p\ {}^2P_{1/2}^{\rm o}$ transition of the singly ionized plasma ions. Fluorescence photons at this same wavelength are collected as a function of time after the plasma is generated using a 1-GHz bandwidth photo-multiplier tube and digital oscilloscope. By varying the detuning of the probe

laser beam we are able to map out the velocity distribution of the Ca^+ ions through the Doppler shift, since the fluorescence signal is a measure of the number of ions in the plasma that are Doppler shifted into resonance with the probe laser beam. At early times the fluorescence signal is dominated by the acceleration of the ions due to DIH, which broadens the velocity distribution. Depending on the probe laser beam detuning, this broadening affects the fluorescence signal differently.

When the probe laser beam is on resonance (blue line in Fig. 1), the fluorescence signal falls rapidly between 25 and 100 ns. The DIH process is the dominant mechanism for broadening the velocity distribution during this time. The signal level falls because fewer ions remain near zero velocity as time goes on. When the probe laser beam is detuned from resonance, DIH-broadening and plasma expansion Doppler-shift ions into resonance with the probe laser beam. Initially there are no ions in resonance with the detuned probe laser beam. However DIH broadens the distribution, causing a corresponding increase in the fluorescence signal that result in the peaks visible in the 30 MHz and 50 MHz detuned data in 1. This peak is often referred to as the DIH peak.

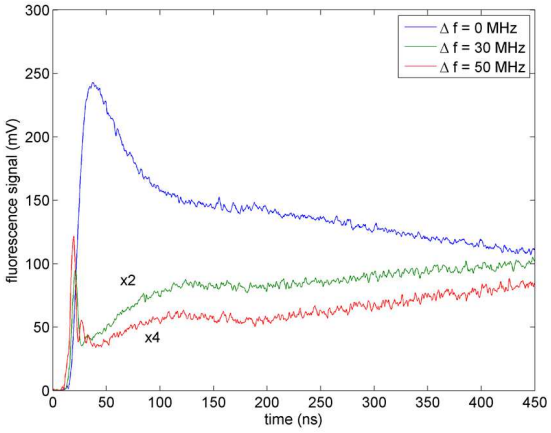

FIG. 2. Typical fluorescence data obtained at three different detunings of the probe laser beam. At non-zero probe laser beam detunings, a heavily damped Rabi oscillation appears in the signal. As the ion velocity distribution broadens due to DIH and plasma expansion, the fluorescence signals change. The shoulder peak visible in the off-resonance plots at about 100 ns is due to DIH and is called the DIH peak.

D. The Ca^{2+} Experiment

Simulations suggest that using a second ionization pulse to promote the ions in the plasmas to a higher ionization state could be used to study the ultrafast dynamics of ultracold plasmas [8]. These simulations, illustrated in Fig. 3, show that the effect that the second ionization pulse has on the energy landscape of the ions depends on their relative positions or, in other words, at what point in time during DIH the second pulse arrives. If the plasma is ionized again at the height of the DIH peak, which corresponds to the greatest spatial ordering, the ion temperature will not change, but the nearest-neighbor potential energy will quadruple. This is illustrated by the red plot in Fig. 3. Quadrupling the potential energy without increasing the kinetic energy effectively quadruples the strong coupling of the system. If the plasma is ionized at some later time it will undergo a second DIH phase, as shown by the green plot if Fig. 3.

Pulse dye lasers, which overlap temporally and spatially, are used to generate the Ca^{2+} plasma. A system was designed and implemented which goes from the $4s\ ^2S_{1/2} \rightarrow 4p\ ^2P^o_{1/2}$ states, at 397 nm, then from $4p\ ^2P^o_{1/2} \rightarrow 5d\ ^2D_{3/2}$, at 210 nm, and finally from $5d\ ^2D_{3/2} \rightarrow$**continuum**, at 355 nm. We achieve narrowband excitation at 397 nm by pulse amplifying and frequency doubling a narrow linewidth injection locked cw diode laser at 794 nm. Similarly, for the 210 nm transition, we pulse amplify and frequency double the output of a narrowband cw laser at 840 nm and then pulse amplify and frequency double again to reach 210 nm. Since the linewidths of the 397 nm and 210 nm transitions are narrow, those transitions do not require much power to saturate. The last step into the continuum requires much more power, which we achieve by using the third harmonic of a pulsed ND:YAG laser at 355 nm.

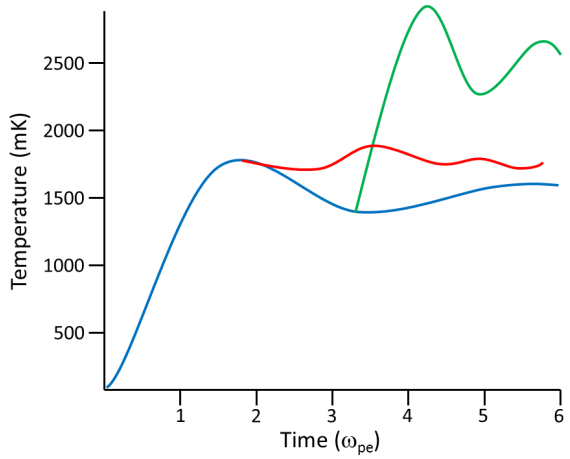

FIG. 3. The simulated ion temperature versus the timing of the second ionization laser pulse. After the plasma is created, the ion temperature rises as the ions undergo DIH and move to minimize their potential energy. The blue plot simulates the ion temperature if the system is not ionized again. The red plot shows that ionizing the plasma again at the height of the DIH peak does not change the ion temperature. The green plot illustrates that if the plasma is ionized again at some later time, the ions will undergo a second DIH phase and the ion temperature will increase.

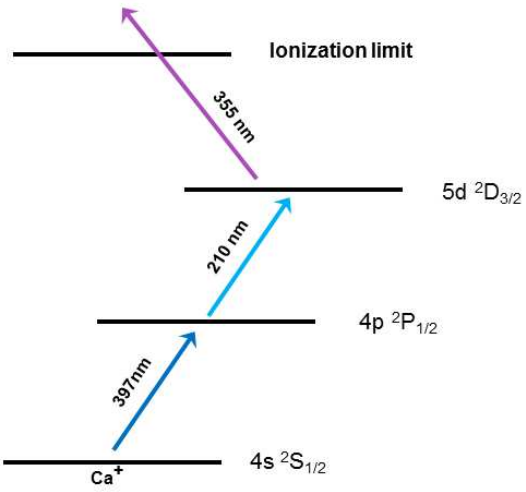

FIG. 4. Partial energy level diagram for Ca^{2+}. The second ionization is achieved in a three photon ionization process. The first step is a narrowband excitation at 397 nm that uses the pulse amplified and frequency doubled output of a narrow linewidth cw laser at 794 nm. The second step is the pulse amplified and frequency quadrupled output of a narrowband cw laser at 840 nm. For the final step we use the third harmonic of a pulsed Nd:YAG laser at 355 nm.

III. Data analysis

A. Fitting to a Voigt profile

We extract the time evolving ion velocity $v_{i,\mathrm{rms}}$ by fitting the fluorescence data to a Voigt profile. The Voigt profile is a mathematical representation of the absorption cross section per atom. It is the convolution of a Lorentzian and a Gaussian lineshape

$$V(\nu) = \int_{-\infty}^{\infty} L(\nu - \nu')G(\nu')d\nu' \qquad (2)$$

with the Lorenztian and Gaussian profiles given by

$$L(\nu) = \frac{\gamma/\pi}{\nu^2 + \gamma^2} \qquad (3)$$

and

$$G(\nu) = \frac{1}{\sqrt{2\pi}\nu_{\mathrm{rms}}} \exp[-\nu^2/2\nu_{\mathrm{rms}}^2], \qquad (4)$$

respectively. In these equations, ν is the detuning from resonance, γ is half the natural linewidth of the atomic transition (the HWHM of the Lorentzian line shape), and ν_{rms} is the rms Gaussian width. The integral defined in Eq. (2) can be evaluated as

$$V(\nu) = \frac{\mathrm{Re}[w(z)]}{\sqrt{2\pi}\nu_{rms}}. \qquad (5)$$

The term in the numerator is the complex error function, and it is given by $w(z) = e^{-z^2}\mathrm{erfc}\,(-iz)$, where z is $(\nu + i\gamma)/\sqrt{2}\nu_{\mathrm{rms}}$, and erfc is the complementary error function. In the analysis, the Lorentzian half width is equal to 11 MHz, half the natural linewidth of the 397 nm transition. The Gaussian width ν_{rms} is extracted as a fit parameter. It is converted to the rms width of the velocity distribution using the Doppler shift, $v_{\mathrm{i,rms}} = (k_{\mathrm{B}}T_i/m_i)^{1/2} = \lambda\nu_{\mathrm{rms}}$, allowing us to map out the width of the ion velocity distribution as a function of time.

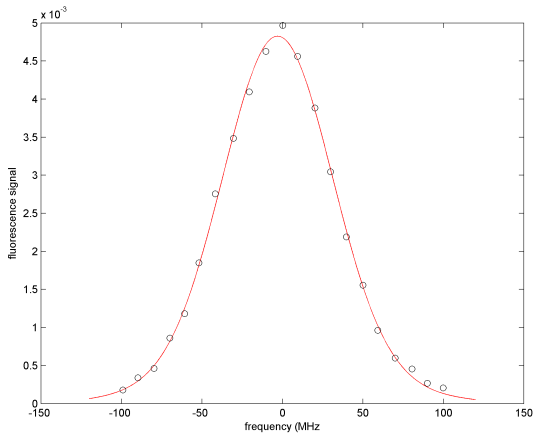

FIG. 5. Fit of experimental data to a Voigt profile. The Voigt profile is the convolution of Lorentzian and Gaussian lineshapes. The Lorentzian half width is half the natural linewidth of the transition and is fixed at 11 Mhz. The Gaussian width is extracted as a fit parameter and is used to find the rms velocity of the ions.

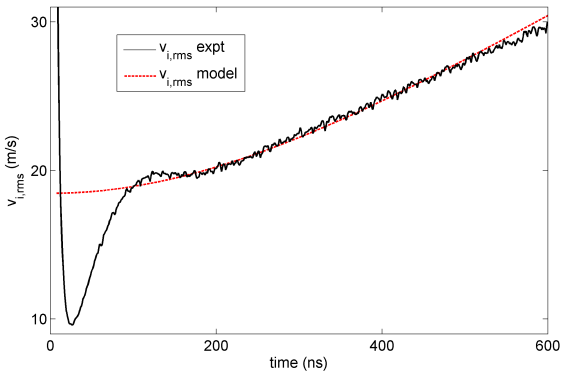

FIG. 6. The time evolving rms width of the ion velocity distribution. The rms velocity width is found using a fit to a Voigt profile, where the Gaussian frequency width is extracted as a fit parameter and converted to the velocity width through the Doppler shift. The model described by Eq. (6) is plotted as the red dashed line.

B. Extracting the ion temperature

Using the $v_{i,\mathrm{rms}}$ found from the Voigt fitting we are able to extract the ion temperature. The ion temperature is determined by the self-similar solution to the Vlasov equations and can be related to the rms ion velocity as [9]

$$v_{i,\mathrm{rms}} = \sqrt{\frac{k_B}{m_i}\left\{\frac{t^2}{\tau_{\mathrm{exp}}^2}[T_e(t)+T_i(t)]+T_i(t)\right\}}, \tag{6}$$

where τ_{exp}, the characteristic expansion time, is given by $\tau_{\mathrm{exp}} = \sqrt{m_i\sigma(0)^2/k_{\mathrm{B}}[T_{\mathrm{e}}(0)+T_{\mathrm{i}}(0)]}$ and the time evolving ion and electron temperatures are given by $T_\alpha(t) = T_\alpha(0)/(1+t^2/\tau_{\mathrm{exp}}^2)$ and the subscript $\alpha = i, e$. In Fig. 6 we have plotted the $v_{i,\mathrm{rms}}$ calculated from this model and the $v_{i,\mathrm{rms}}$ found by fitting a Voigt profile to the fluorescence data of one of our plasmas. Rearranging Eq. (6) we solve for the ion temperature $T_i(t)$

$$T_i(t) = \frac{m_i v_{\mathrm{i,rms}}^2}{k_B} - \frac{T_e(0)\frac{t^2}{\tau_{\mathrm{exp}}^2}}{1+\frac{t^2}{\tau_{\mathrm{exp}}^2}} \tag{7}$$

IV. Experimental results

Using the methods described in the previous sections, we have made measurements of the Ca^+ fluorescence for different timings of the second ionization pulses relative to the first ionization pulses. Fitting these fluorescence measurements to a Voigt profile, as described in Sec.III A, allows us to find the time-evolving rms velocity of the Ca^+ ions, as shown in Fig. 7. The gaps that appear in the data occur at the time in which the second ionization pulses arrive. At this time the scattered light from the pulses make it difficult to extract a meaningful velocity width from the fluorescence measurements. This necessitates using other means to determine the change in the temperature of the Ca^+ ions due to the Ca^{2+} ions.

In order to determine the change in the Ca^+ temperature we will need to compare the data from the plasmas that undergo the second ionization process to a plasma that is just singly ionized. We will fit the ion velocity distribution from the singly ionized plasma to the model described in Sec.III B. The model will then be subtracted from the velocity distribution of a partially doubly ionized plasma in order to subtract

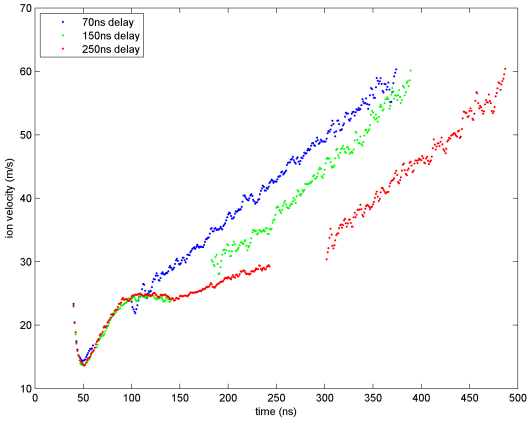

FIG. 7. The rms velocity of the Ca^+ ions in a plasma that has been partially doubly ionized. The three different lines correspond to three different timings of the second ionization laser pulses. It is apparent that the timing of the second ionization pulse has a dramatic effect on the velocity of the Ca^+ ions.

off the contribution from the expansion of the plasma. What is left is the contribution to the velocity distribution that comes from the influence of the Ca^{2+} ions on the Ca^+ ions. This can be fit to the model described by Eq. 6 in order to find the change in the Ca^+ ion temperature due to the second ionization. Once we have the change in the ion temperature we can calculate the strong coupling of the plasma. This work is presently underway.

V. Conclusion

We have built an experiment in laser-cooled calcium designed to test the prediction that higher values of the strong coupling parameter in ultracold neutral plasmas can be realized if the plasma ions are excited to higher ionization states. Using laser-induced fluorescence we map out the ion velocity distribution of the singly ionized Ca in order to measure the effect that the timing of second ionization pulses has on the temperature of the Ca^+ ions. Future work includes determining the change in the Ca^+ ion temperature and in the ion strong coupling due to the second ionization.

VI. Acknowledgments

This work is supported in part by the National Science Foundation (grant no PHY-0969856), the Air Force Office of Scientific Research (grant no. FA9950-12-1-0308) and NASA (Utah Space Grant Consortium).

[1] Y. C. Chen, C. E. Simien, S. Laha, P. Gupta, Y. N. Martinez, P. G. Mickelson, S. B. Nagel, and T. C. Killian, "Electron Screening and Kinetic-Energy Oscillations in a Strongly Coupled Plasma," Phys. Rev. Lett. 93, 265003 (2004).

[2] M. S. Murillo, "Ultrafast Dynamics of Strongly Coupled Plasmas," Phys. Rev. Lett. 96, 165001 (2006).

[3] S. Laha, Y. C. Chen, P. Gupta, C. E. Simien, Y. N. Martinez, P. G. Mickelson, S. B. Nagel, and T. C. Killian, "Kinetic energy oscillations in annular regions of ultracold neutral plasmas," Eur. Phys. J. D pp. 5156 (2006).

[4] J. Castro, P. McQuillen, H. Gao, and T. C. Killian, "The role of collisions and strong coupling in ultracold plasmas," Journal of Physics: Conference Series 194, 012065 (2009).

[5] S. D. Bergeson, A. Denning, M. Lyon, and F. Robicheaux, "Density and temperature scaling of disorder-induced heating in ultracold plasmas," Phys. Rev. A **83**, 023409 (2011).

[6] M. S. Murillo, "Ultrafast phase-space dynamics of ultracold, neutral plasmas," J. Phy. A **42**, 214054 (2009)

[7] E. A. Cummings, J. E. Daily, D. S. Durfee, and S. D. Bergeson, "Fluorescence measurements of expanding strongly coupled neutral plasmas," Phys. Rev. Lett. 95, 235001 (2005).

[8] M. S. Murillo, "Ultrafast dynamics of neutral, ultracold plasmas," Physics of Plasmas 14, 055702 (2007).

[9] M. Lyon, S. D. Bergeson, and M. S. Murillo, "Limit of strong ion coupling due to electron shielding,"Phys. Rev. E 87, 033101 (2013).